

# Effect of nanocrystallization on the structural and electrical conductivity enhancement of vanadium-based glasses

O. A. AL-Hartomy · A. A. Al-Ghamdi ·  
F. EL-Tantawy · M. M. El-Desoky

Received: 5 June 2012 / Accepted: 8 December 2012 / Published online: 20 December 2012  
© Springer Science+Business Media New York 2012

**Abstract** A new glass–ceramic nanocomposites material was prepared by a thermal nanocrystallization of  $V_2O_5$ – $Bi_2O_3$ – $P_2O_5$  system with different  $V_2O_5$  content. The amorphous state of glassy materials is confirmed by X-ray diffraction. It was shown by XRD and SEM studies that by suitable heat-treatment glasses can be turned into glass–ceramic nanocomposites consisting of crystallites smaller than 80 nm inserted in the glassy matrix. Also, it was shown that thermal nanocrystallization of as-prepared glassy samples leads to creation of nanocrystalline grains of  $V_2O_5$ ,  $Bi_2O_3$ , and  $BiVO_4$  phases. The glass–ceramic nanocomposites obtained show giant enhancement of electrical conductivity than the as-prepared glasses. The conductivity enhancement was recognized to interfacial regions adjacent crystalline grains. The conduction of the present glasses and their glass–ceramic nanocomposites was confirmed to be due to primarily non-adiabatic hopping of small polaron between vanadium ions.

## Introduction

Glass–ceramic materials with the grain size of crystallites smaller than 100 nm (nanocrystallites) are still glasses and show exclusive properties [1–3]. However, the manufacture of nanocrystals is a very significant subject for the development of nanotechnology. A glass is identified to crystallize through the nucleation and development procedure during thermal nanocrystallization [1]. These materials can be achieved by technique of thermal nanocrystallization of glasses. In the thermal nanocrystallization, a structure of nanocrystals distributed in the glass matrix, so-called glass–ceramic nanocomposites [1, 2] is prepared, and unexpected functionalities because of the existence of nanocrystals have been reported lately [2–12]. The main feature of these glass–ceramic nanocomposites containing transition metal oxides (TMO), is its lower level of porosity when compared to that of the ceramics [13, 14]. However, this technique is inexpensive and potentially meet for multifunctional devices [14].

On the other hand, the electrical properties of TMO glass–ceramics nanocomposites arise from the existence of different valence states of TMO [13–17]. In these nanomaterials the electrical conductivity is due to the transport of electrons or polarons. The conduction mechanism of these materials was discussed by the small polaron hopping (SPH) model [18, 19]. In addition, glass–ceramics nanocomposites with high content of  $V_2O_5$  show considerable electronic conduction [17]. Purely electronic conducting glasses can be employed as cathode materials in unique advanced electrochemical cells [14]. Electrical conductivity of TMO glass systems can be enhanced by nanocrystallization [13, 17]. The conductivity improvement caused by the existence of nanocrystalline grains is generally ascribed to creation of extremely defective regions around the grains.

---

O. A. AL-Hartomy  
Department of Physics, Faculty of Science, Tabuk University,  
Tabuk 71491, Saudi Arabia

A. A. Al-Ghamdi  
Department of Physics, Faculty of Science, King Abdulaziz  
University, Jeddah 21589, Saudi Arabia

F. EL-Tantawy  
Department of Physics, Faculty of Science, Suez Canal  
University, Ismailia, Egypt

M. M. El-Desoky (✉)  
Department of Physics, Faculty of Science, Suez University,  
Suez, Egypt  
e-mail: mmdesoky@gmail.com

The main aim of this study was to prepare and characterize materials of the  $V_2O_5$ – $Bi_2O_3$ – $P_2O_5$  glasses and its glass–ceramic nanocomposites showing enhanced electrical conductivity compared to those of the as-prepared glasses. Glass–ceramic nanocomposites, where made by annealing glasses under study at temperatures close to crystallization temperature.

### Experimental technique

A series of vitreous samples of approximate composition  $xV_2O_5$ – $20Bi_2O_3$ – $(x-100)P_2O_5$  for  $10 \leq x \leq 50$  were synthesized by a press-quenching technique. Reagent grade  $P_2O_5$  (99.99 %),  $Bi_2O_3$  (99.999 %), and  $V_2O_5$  (99.99 %) were used as raw materials. After mixing in air a batch 20 g with prescribed compositions in platinum crucible, the mixture were melted in the temperature range 1150–1200 °C depending on the compositions for 1 h. The glass–ceramic nanocomposites were obtained by crystallization glasses at temperatures near crystallization temperature for 2 h in air.

DSC runs were carried out for ground glass batches of about 120 mg in air atmosphere using Shimatzou DSC 50 instrument with a heating rate  $15 \text{ }^\circ\text{C min}^{-1}$  in the temperature range from room temperature to 650 °C. X-ray diffractometry (XRD) measurements carried out using a Shimatzou XRD-6000. The scanning electron micrograph (SEM) measurements were carried using JEOLI-5800LV.

Archimedes principle with toluene as an immersion liquid was used to measure the density of the samples. The concentration of vanadium ions,  $N \text{ (cm}^{-3}\text{)}$  was estimated using  $N = dpN_A/(A_w \times 100)$ , where  $d$  is the density of the sample,  $N_A$  is the Avogadro constant,  $p$  is the weight percentage of atoms, and  $A_w$  is the atomic weight. The dc electrical conductivity ( $\sigma$ ) were measured using multimeter type Keithley 760 at temperatures between 313 and 523 K. Silver paste electrodes put on both faces of the polished glasses and their glass–ceramic nanocomposites samples.

### Results and discussion

#### DSC

Figure 1 shows DSC for  $60V_2O_5$ – $20P_2O_5$ – $20Bi_2O_3$  glass and the composition dependence of glass transition temperature ( $T_g$ ), crystallization temperature ( $T_c$ ), and temperature difference  $\Delta T = T_c - T_g$ , respectively, for the present glass system. All curves exhibit an endothermic dip due to  $T_g$  and exothermic peak corresponding to crystallization ( $T_c$ ). Also from the figure, it is clear that  $T_g$

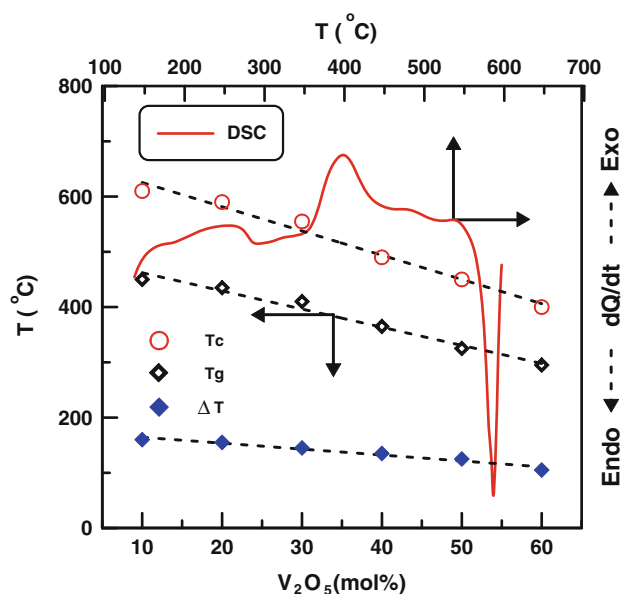


**Fig. 1** DSC thermogram for  $60V_2O_5$ – $20P_2O_5$ – $20Bi_2O_3$  glass and composition dependence of glass transition temperature ( $T_g$ ), crystallization temperature ( $T_c$ ), and temperature difference ( $\Delta T$ ) for different glass compositions

decreases with increasing  $V_2O_5$  content and lies between 295 and 450 °C. Moreover,  $T_c$  lies between 400 and 610 °C for the present system. It is known that the thermal stability of a glass depends on the temperature difference  $\Delta T = T_c - T_g$  of the glasses [13–17]. The average difference value between  $T_g$  and  $T_c$  is about 132 °C and it decreases with the increase of  $V_2O_5$  content indicating that the thermal stability of the glasses decreases with  $V_2O_5$  content. Since these glasses are greatly viscous and  $\Delta T$  is quite large, many forms such as wires, tapes can be synthesized from viscous metals.

On the other hand, DSC studies [18] on the structural of several glasses have already showed that  $T_g$  shows an clear correlation with the change in the coordination number of the network former and the creation of non-bridging oxygen (NBO) atoms, which means destruction of the network structural [18]. Usually,  $T_g$  shows a clear increase while the coordination number of the network former increases. Converse to this, a creation of NBO causes a decrease into the  $T_g$ . The continuous decrease in the  $T_g$  in the current system, therefore, seems to advise continuing increase in the coordination number of  $V^{5+}$  and  $V^{4+}$  ions and creation of NBO atoms [16, 17]. Also, the decrease in  $T_g$  advises that the strength of the chemical bond between metal and oxygen atoms becomes weakened. This is attributed to the increased interatomic distances between metal and oxygen ions leading to increase in the oxygen molar volume and decrease in the density [18].

XRD

Figure 2a, b shows XRD patterns of present glasses and its glass–ceramic nanocomposites, respectively. In the first case of glass sample (Fig. 2a) there is only a broad halo detected with no indication of diffraction peaks. This approves the amorphous state of early glasses. Pattern shown in Fig. 2b were collected for samples after its heat-treatment temperatures near to  $T_c$  for 2 h, determined from DSC studies. It contains a number of diffraction peaks

consistent to a nanocrystalline  $V_2O_5$ ,  $Bi_2O_3$ , and  $BiVO_4$  phases. XRD pattern in Fig. 2b is a strong indication that heat-treatment temperature  $T_c$  only starts to create small nanocrystallites implanted in the glass matrix [16, 17]. This is a valuable hint, since it means that by controlling the heat-treatment temperature, one can control the quantity of nanocrystalline grains formed in the glass matrix and thus improve its electrical conductivity (see next “DC conductivity” section). The nanocrystallization processes and relationship between the processes and conductivity enhancement will be discussed in detailed in our future paper.

Furthermore, there are some new peaks consistent to the phase which we have not recognized yet. The mean particle sizes,  $D$ , of the precipitated nanocrystals in the glassy matrix were determined according to Sherrer’s equation;

$$D = \frac{k\lambda}{\beta \cos \theta} \tag{1}$$

$D$  was found to be about  $60 \pm 3.0$  nm for all present samples, where  $\theta$  is the Bragg angle of XRD peak,  $k \sim 1$ ,  $\lambda$  (nm) represents the wavelength of Cu  $K\alpha$  radiation and  $\beta$  represents the modified full width at half maximum of the diffraction peak in radians. The specified particle size is the average as obtained by means of applying Sherrer’s equation on all Bragg’s peaks resultant to  $V_2O_5$  presented in the XRD pattern, e.g., Fig. 2b.

SEM

To additional understand the structure of these samples microstructural study of these materials was performed by scanning electron microscopy (SEM). Figure 3a, b shows SEM of  $60V_2O_5-20P_2O_5-20Bi_2O_3$  glass and its heat treated sample, respectively. In this figure one can see a surface nearly without the existence of microstructure, which is a characteristic of obvious precipitation indicating a glassy phase. Nevertheless, SEM picture (Fig. 3b) of  $60V_2O_5-20P_2O_5-20Bi_2O_3$  heated sample at  $T_c$  for 2 h, shows the existence of many nanocrystallites (average size of 40–80 nm). Besides nanocrystallites one can see some remnant amorphous phase. In our opinion, such existence of nanocrystalline and amorphous phase shows a crucial role in forming of easy conduction paths for hopping of electron [14, 15].

Density and molar volume

The density,  $d$ , and molar volume,  $V_m$ , as a function of  $V_2O_5$  content for the present glasses and its glass–ceramic nanocomposites are shown in Fig. 4 and Tables 1 and 2. These properties changed linearly as a function of glass composition. From the figure, it may be observed that

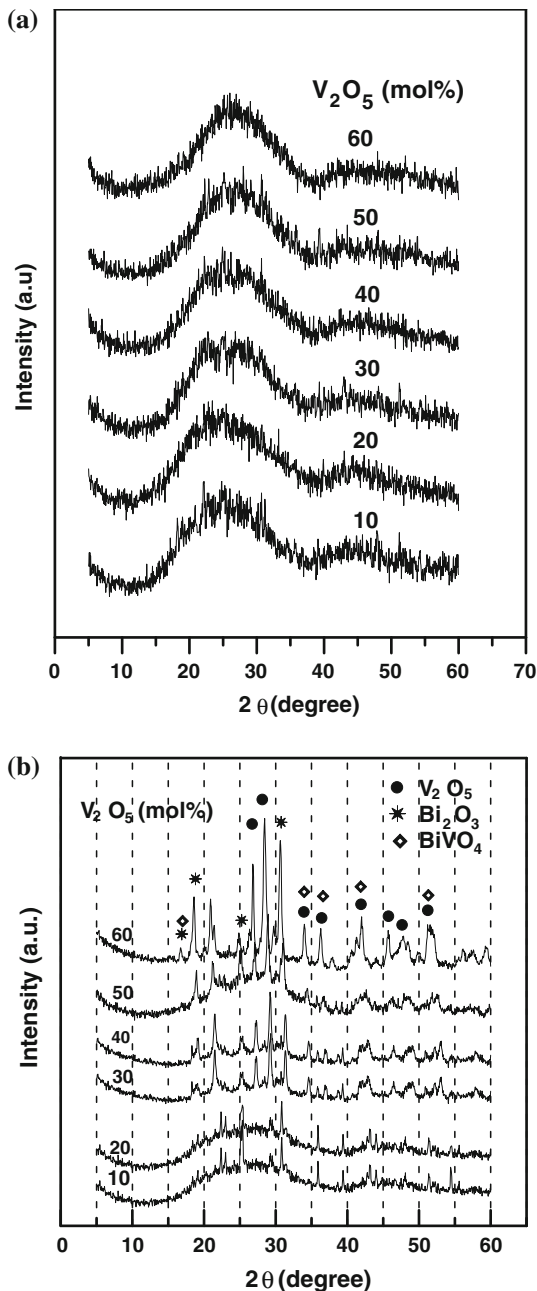
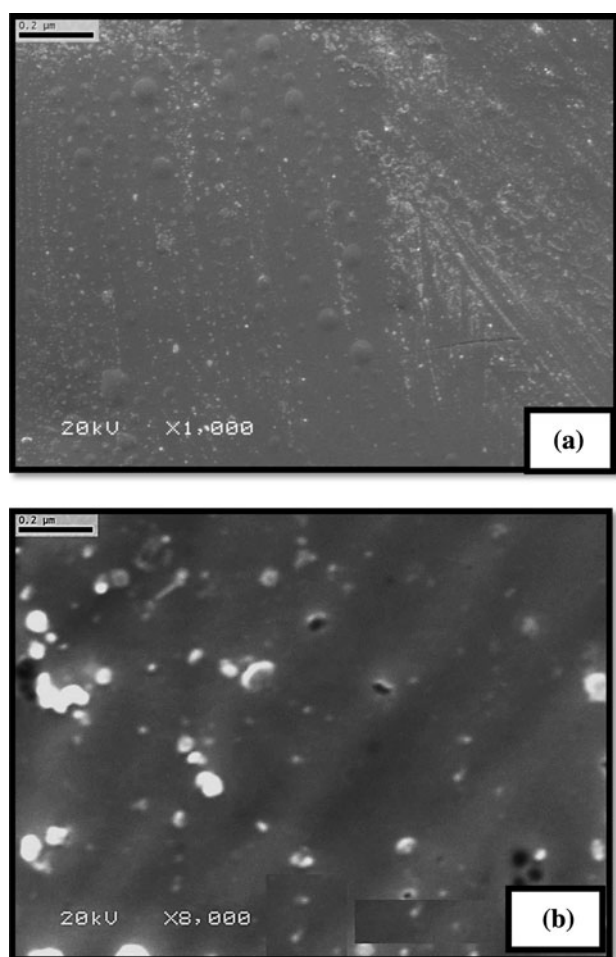


Fig. 2 X-ray diffraction for a  $V_2O_5-P_2O_5-Bi_2O_3$  glasses and b their glass–ceramic nanocomposites



**Fig. 3** SEM for for **a** 60V<sub>2</sub>O<sub>5</sub>–20P<sub>2</sub>O<sub>5</sub>–20Bi<sub>2</sub>O<sub>3</sub> glasses and **b** their glass–ceramic nanocomposites

density ( $d$ ) decreases regularly with the increase of the V<sub>2</sub>O<sub>5</sub> content. The density results appearance that has the vanadium cation content increases the glass structure which develops more open, allowing for the probable creation of increasing number of NBO [17]. Also, it is found that the molar volume increases with increasing vanadium cation concentration; this may be due to the result of the polarizing power strength, PPS, which is a measure of ratio of the cation valance and their diameter. The PPS of phosphorous cation is lower than that of, vanadium cation which causes the packing fraction to subsequently decrease due to more attracting force of vanadium cations to oxygen anions. In these current samples the densities vary from 3.76 to 4.47 g cm<sup>-3</sup> and 3.83 to 4.53 g cm<sup>-3</sup> for glasses and its glass–ceramic nanocomposites, respectively. It is clear that these glass–ceramic nanocomposites exhibit high density compared to the samples in glassy state. Here the dependence of composition of molar volume gives evidence about the coordination state of the vanadium cations. The obvious increase of

molar volume suggests that phosphorous cations have a small coordination number of phosphorous atoms would cause an increase of molar volume [19–22]. However, the molar volume and density for this system are consistent with the atomic weight, ionic size, and quantity of different elements in the glasses [21, 23].

#### DC conductivity

The dc electrical conductivity,  $\sigma$ , as a function of inverse temperature of the present glasses and their glass–ceramic nanocomposites are shown in Fig. 5a, b, respectively. It is showed that from the figure linear temperature dependence up to a definite temperature  $\theta_D/2$  ( $\theta_D$  Debye temperature). Similar behavior arises from the hopping of electrons or polarons between different valance states (e.g., V<sup>4+</sup>, V<sup>5+</sup>) [13–17]. The experimental electrical conductivity results at high temperature were fitted with SPH model suggested by Mott [19, 20]. The activation energy at high temperature was determined from the slope of each curve. The electrical conductivity data is well-defined by activation energy for conduction known by Mott equation. [19, 20].

$$\sigma = \sigma_0 \exp(-W/kT) \quad (2)$$

where  $W$  is the activation energy,  $\sigma_0$  is a pre-exponential factor and  $k$  is the Boltzmann constant. The variation of activation energy and electrical conductivity of present glasses and its glass–ceramic nanocomposites with different composition are shown in Fig. 6. From the figure it is clear that the conductivity decreases while the activation energy increases with the increase of the V<sub>2</sub>O<sub>5</sub> content. Such a behavior is a feature of SPH [20, 21]. The low value of electrical conductivity and high value of activation energy are similar to those for our recent papers of glass–ceramic nanocrystals containing vanadium oxides [22, 24]. This change in activation energy and electrical conductivity may aid to identify the structural variations as a result of increasing V<sub>2</sub>O<sub>5</sub> content.

The variation of electrical conductivity as a function of V<sub>2</sub>O<sub>5</sub> content at a fixed temperature (350 K) of glasses and their glass–ceramic nanocomposites are shown in Fig. 7. From the figure it is clear that these glass–ceramic nanocomposites exhibit high electrical conductivity compared to the samples in glassy state [1–9]. The improvement of electrical conductivity of this case is considered to be due to the existence of nanocrystals in the glass matrix with an average grain size of 60 nm as reported in XRD and SEM results. Similar remarkable increases in conductivity have been reported in recent papers of glass–ceramic nanocomposites containing vanadium oxides [22, 24]. With an enhancement in electrical conductivity by nanocrystallization, the activation energies for conduction were found to be  $W_{\text{nano}} = 0.34\text{--}0.51$  eV at high temperatures for glass–ceramics

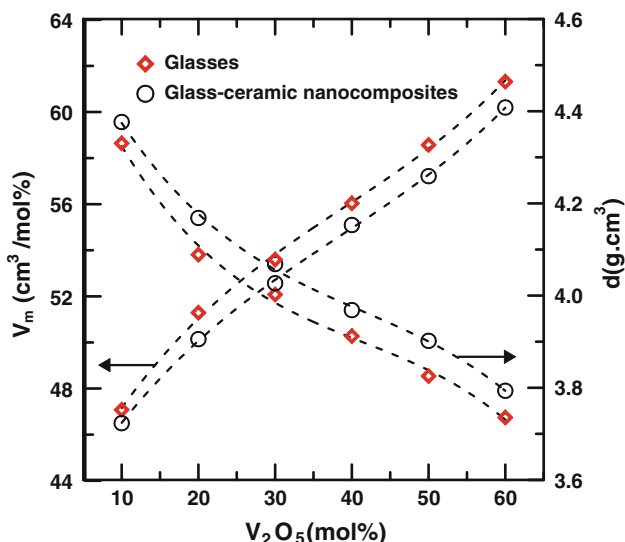


**Fig. 4** Composition dependence of density ( $d$ ) and oxygen molar volume ( $V_m$ ) for  $V_2O_5$ - $P_2O_5$ - $Bi_2O_3$  glasses and their glass-ceramic nanocomposites

nanocomposites which are much lower than those for the as-prepared glasses  $W_{\text{glass}} = 0.39$ – $0.57$  eV at high temperatures (Tables 1, 2). However, it is well-known that the addition of  $V_2O_5$  to glass or glass-ceramic nanocomposites increases the electrical conductivity as a result of increasing number of NBO cations [17, 22, 24].

The improvement of electrical conductivity of these glass-ceramic nanocomposites can be described in the following way. The electronic conduction mechanism in the glasses of the  $V_2O_5$ - $Bi_2O_3$ - $P_2O_5$  system with high quantity of  $V_2O_5$  is the spatial distribution of  $V^{4+}$  and  $V^{5+}$  ions which are centers of hopping conduction of polaron [1–9]. The heat treatment at temperatures near to  $T_c$  leads to the creation of  $V_2O_5$  nanocrystallites embedded in the glass matrix. Subsequently, the average grain size is about 60 nm, the interface between crystalline and glass matrix is very widely ramified and strongly effects overall electrical conductivity properties of the nanomaterial as described in SEM and XRD. Especially, it may contain the enhanced  $V^{4+}$  and  $V^{5+}$  centers dispersed on the surface of  $V_2O_5$  nanocrystallites [5–9]. However, this significant improvement of electrical conductivity after heat treatment is attributed to creation of extensive and dense network of electronic easy conduction paths which are situated between  $V_2O_5$  nanocrystals and on its surfaces [13, 17].

Furthermore, the decrease in activation energy and increase in electrical conductivity (Fig. 6) for the present samples glass and its glass-ceramic nanocomposites lead to changes in mechanism of conduction. In addition, glass and glass-ceramic nanocomposites containing  $V_2O_5$  exhibit considerable electronic conduction [13–17] and depends strongly upon the average distance,  $R$ , between vanadium ions. The mean spacing between the V ions,  $R$ ,

**Table 1** Chemical composition, physical properties, and SPH parameters of  $V_2O_5$ - $Bi_2O_3$ - $P_2O_5$  glasses

Nominal composition (mol%)			$d \pm 0.002$ (g cm <sup>-3</sup> )	$W_{\text{glass}} \pm 0.01$ (eV)	$\log \sigma \pm 0.02$ (at 450 K) (S m <sup>-1</sup> )	$R \pm 0.001$ (nm)	$N \pm 0.001$ ( $\times 10^{22}$ cm <sup>-3</sup> )	$r_p \pm 0.001$ (nm)	$N(E_F) (\times 10^{21})$ (eV <sup>-1</sup> cm <sup>-3</sup> )
$V_2O_5$	$P_2O_5$	$Bi_2O_3$							
10	70	20	4.476	0.57	-8.31	0.428	1.279	0.172	5.35
20	60	20	4.186	0.47	-7.62	0.439	1.174	0.177	5.96
30	50	20	4.082	0.45	-7.23	0.447	1.123	0.179	5.97
40	40	20	3.974	0.44	-6.18	0.453	1.074	0.182	5.83
50	30	20	3.870	0.42	-5.61	0.459	1.028	0.185	5.84
60	20	20	3.762	0.39	-5.11	0.466	0.098	0.188	6.02

**Table 2** Chemical composition, physical properties, and SPH parameters of  $V_2O_5$ - $Bi_2O_3$ - $P_2O_5$  glass-ceramic nanocomposites

Nominal composition (mol%)			$d \pm 0.002$ (g cm <sup>-3</sup> )	$W_{\text{nano}} \pm 0.01$ (eV)	$\log \sigma \pm 0.002$ (at 450 K) (S m <sup>-1</sup> )	$R \pm 0.001$ (nm)	$N \pm 0.001$ ( $\times 10^{22}$ cm <sup>-3</sup> )	$r_p \pm 0.001$ (nm)	$N(E_F) (\times 10^{21})$ (eV <sup>-1</sup> cm <sup>-3</sup> )
$V_2O_5$	$P_2O_5$	$Bi_2O_3$							
10	70	20	4.532	0.51	-4.69	0.426	1.195	0.171	6.06
20	60	20	4.282	0.45	-3.77	0.436	1.201	0.176	6.37
30	50	20	4.162	0.42	-3.04	0.444	1.145	0.178	6.51
40	40	20	4.042	0.40	-2.67	0.451	1.093	0.181	6.52
50	30	20	3.962	0.37	-1.97	0.456	1.052	0.184	6.78
60	20	20	3.832	0.34	-1.11	0.464	1.000	0.187	7.03

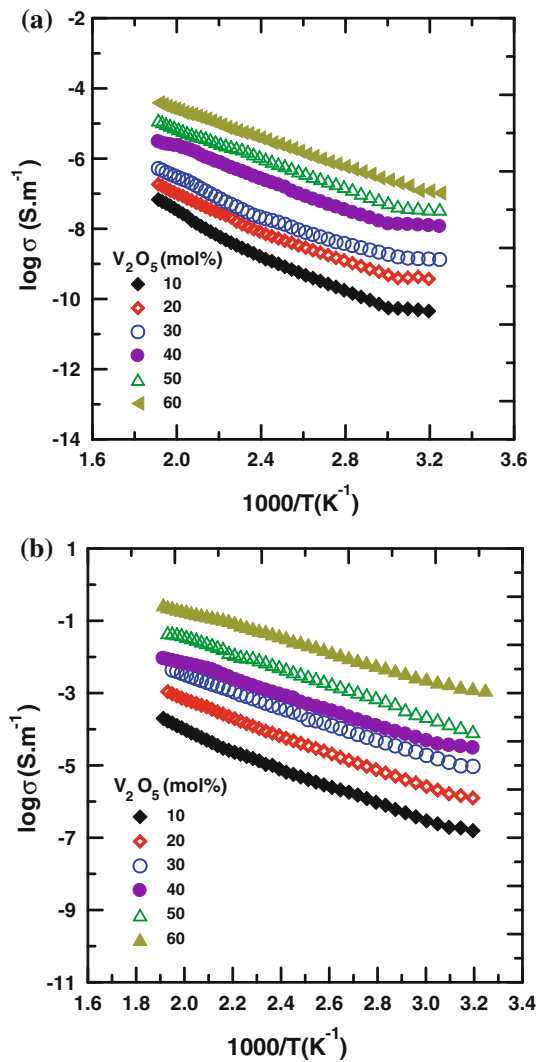


**Fig. 5** Temperature dependence of dc conductivity ( $\sigma$ ) as a function of  $V_2O_5$  content for **a**  $V_2O_5$ - $P_2O_5$ - $Bi_2O_3$  glasses and **b** their glass-ceramic nanocomposites

was determined for the present glass and its glass-ceramic nanocomposites samples from the relation  $R = (1/N)^{1/3}$ , where  $N$  is the concentration of vanadium ions per unit volume (see Tables 1, 2). The relation between the mean spacing between V ions,  $R$ , and activation energy,  $W$ , for the present system is illustrated in Fig. 8. This results shows that there is a prominent positive correlation between  $W$  and  $R$  between transition metal ions. These results agree well with the results suggested by Sayer and Mansingh [21] delineated the dependence of  $W$  on the mean distance between transition metal ions.

The electrical conductivity due to SPH, is given by Mott [19, 20] in the non-adiabatic hopping mechanism as

$$\sigma = \frac{v_0 N e^2 R^2}{kT} C(1 - C) \exp(-2\alpha R) \exp(-W/kT) \quad (3)$$

The pre-exponential factor ( $\sigma_0$ ) in Eq. (3) is given by

$$\sigma_0 = \frac{v_0 N e^2 R^2}{kT} C(1 - C) \exp(-2\alpha R) \quad (4)$$

where  $v_0$  is the optical phonon frequency,  $\alpha$  is the tunneling factor (the ratio of wave function decay),  $N$  is the transition metal density,  $C$  is the TMO ratio fraction of reduced transition metal ion, and  $W$  is the activation energy for hopping conduction. The SPH model based on strong electron-phonon interaction, Austin and Mott [19] have shown that:

$$W = W_H + W_D/2 \quad (\text{for } T > \theta_D/2) \quad (5a)$$

$$W = W_D \quad (\text{for } T < \theta_D/4) \quad (5b)$$

where  $W_D$  is the disorder energy and  $W_H$  is the polaron hopping energy.

The nature of conduction mechanism (adiabatic or non-adiabatic polaron hopping), of this system can be estimated from an experimental relation between  $\log \sigma$  and  $W$  at  $T = 450$  K (Fig. 9) [13, 17]. It is expected that the hopping will be in the adiabatic regime if the temperature estimated  $T_e$ , from the slope of such a plot, is close to the experimental temperature  $T$ . Otherwise the hopping will be in the non-adiabatic regime. From the plot of  $\ln \sigma$  against  $W$  at  $T = 450$  K as shown in Fig. 9, the experimental slopes were not equal to the theoretical slopes. The equivalent temperature ( $T_e$ ) estimated from the experimental slopes were  $T_e = 239$  and  $278$  K for glasses and its glass-ceramic nanocomposites, respectively, which was lower than that of the experimental temperature ( $T = 450$  K). This confirms non-adiabatic hopping of small polaron of the present samples. Figure 10 shows the influence of  $V_2O_5$  content on  $\sigma_0$  indicating an increase in  $\sigma_0$  with  $V_2O_5$  content. It can be concluded again that the conduction mechanism in the present glasses and their glass-ceramic nanocomposites is due to the non-adiabatic hopping of small polarons [17].

Based on a number of investigations Holstein [25] has suggests a method for estimating the polaron hopping energy  $W_H$  as;

$$W_H = (1/4N) \sum_p [\gamma_p]^2 \hbar \omega_p \quad (6)$$

where  $\omega_p$  is the optical phonons frequency and  $[\gamma_p]^2$  is the electron-phonon coupling constant. However, the polaron radius,  $r_p$ , can be evaluated using Bogomolov et al. formula [26]

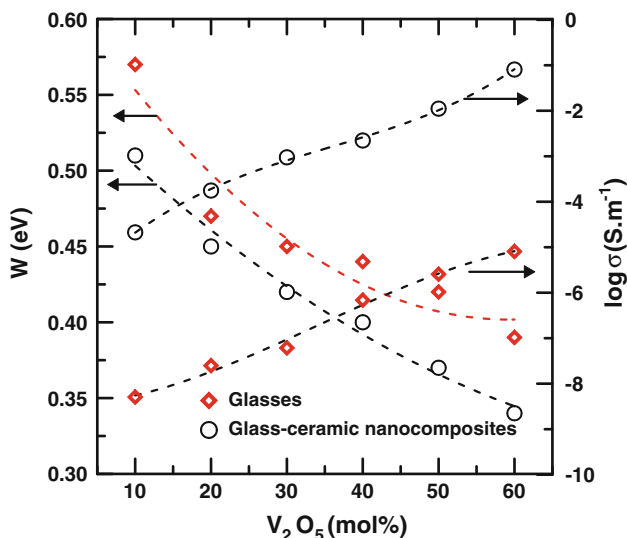


**Fig. 6** The relation between conductivity at 450 K and activation energy as a function of  $V_2O_5$  content for glasses and its glass–ceramic nanocomposites

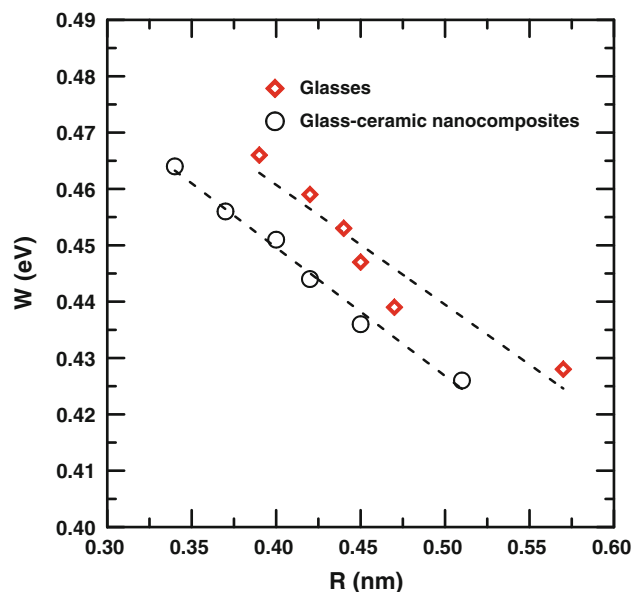


**Fig. 8** Effect of average distance ( $R$ ) on activation energy ( $W$ ) for different glasses and its glass–ceramic nanocomposites

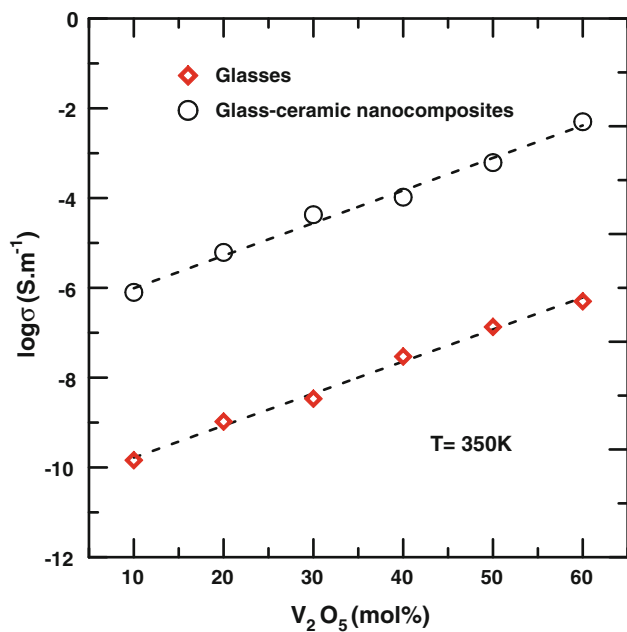


**Fig. 7** Effect of  $V_2O_5$  content on dc conductivity ( $\sigma$ ) at 350 K for different glasses and their glass–ceramic nanocomposites

$$r_p = \left(\frac{\pi}{6}\right)^{1/3} \frac{R}{2} \tag{7}$$

The polaron radii values of the present glasses and its glass–ceramics nanocomposites are listed in Tables 1 and 2, respectively. The small values of polaron radii in both tables suggest that the polarons are highly localized.

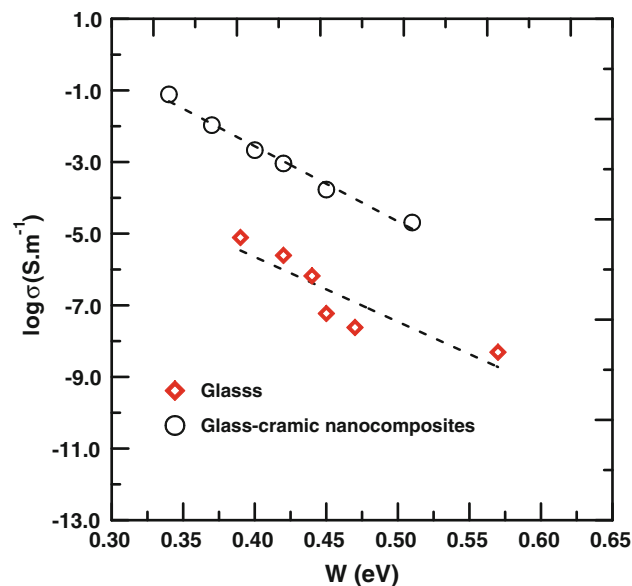


**Fig. 9** Effect of activation energy ( $W$ ) on dc conductivity ( $\sigma$ ) at  $T = 450$  K for different glasses and its glass–ceramic nanocomposites

Finally, we determine the density of states for thermally activated electron hopping close to the Fermi level is estimated as [26]

$$N(E_F) = (3/4\pi R^3 W) \tag{8}$$

The  $N(E_F)$  values for the glasses and its glass–ceramic nanocomposites are given in Tables 1 and 2. These values

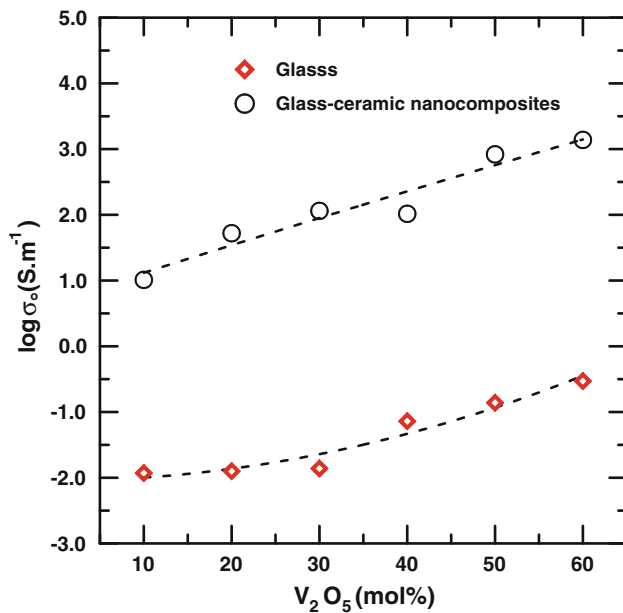


**Fig. 10** Effect of V<sub>2</sub>O<sub>5</sub> content on pre-exponential factor ( $\sigma_0$ ) for different glasses and its glass–ceramic nanocomposites

for glasses and its glass–ceramic nanocomposites are reasonable for localized states [13, 17].

Finally, all the calculated parameters in Tables 1 and 2 depend on the density of glasses and its glass–ceramic nanocomposites. The enhancements of electrical conductivity of glass–ceramic nanocomposites are consistent with high values of density and low values of  $W_{\text{nano}}$ ,  $R$ ,  $N$ , and  $r_p$  [17, 18, 22, 24].

## Conclusion

The V<sub>2</sub>O<sub>5</sub>–P<sub>2</sub>O<sub>5</sub>–Bi<sub>2</sub>O<sub>3</sub> glassy samples have converted into glass–ceramic nanocomposites by heat treatment at crystallization temperature  $T_c$  for 2 h. XRD and SEM of the glass–ceramic nanocomposites show that nanocrystals were implanted in the glassy matrix. After heat treatment they contain nanocrystallites implanted in amorphous matrix with an average grain size of 60 nm. The crystallization temperature  $T_c$  decreases with increasing V<sub>2</sub>O<sub>5</sub> content. The resulting glass–ceramic nanocomposites show much higher electrical conductivity than the as-quenched glasses. It was suggested that the main role in the conductivity improvement of these glass–ceramic nanocomposites is played by the developed interfacial regions between crystalline and glassy matrix, in which the V<sup>4+</sup>–V<sup>5+</sup> pairs concentration responsible for hopping of

electron, has much higher than that inside the glassy matrix. From the best fits of electrical conductivity results, reasonable values of various SPH parameters were obtained. The conduction mechanism of the present samples was attributed to non-adiabatic hopping of small polaron.

**Acknowledgements** The present study is a result of an international cooperation program between University of Tabuk, Tabuk, Saudi Arabia and Suez University, Egypt. The authors gratefully acknowledge the financial support from the University of Tabuk, Project number 0145-1433-S.

## References

- Kingery WD, Bowen HK, Uhlmann DR (1976) Introduction to ceramics, 2nd edn. Wiley, New York, p 320
- Hirao K (2003) Bull Ceram Soc Jpn 38:323
- Tamagawa N, Benino Y, Fujiwara T, Komatsu T (2003) Opt Commun 217:387
- Honma T, Benino Y, Fujiwara T, Komatsu T, Sato R (2002) Opt Mater 33:27
- Senthil Murugan G, Varma KBR (2002) J Mater Chem 12:1426
- Torres F, Benito Y, Komatsu T, Lavelle C (2001) J Mater Sci 36:4961. doi:10.1023/A:1011808926424
- Sigaev VN, Akimova OV, Pernice P, Aronne A, Yu Stefanovich S, Scaglione A (2001) J Non Cryst Solid 292:59
- Zhou ZH, Wang J, Xue JM, Chan HSO (2001) Appl Phys Lett 79:316
- Hirano K, Benino Y, Komatsu T (2001) J Phys Chem Solids 62:2075
- Syam Prasad N, Varma KBR, Lang SB (2001) J Phys Chem Solids 62:1299
- Frenkel AI, Kolobov AV, Robinson IK, Cross JO, Maeda Y, Bouldin CE (2002) Phys Rev Lett 89:285503
- Ghigna P, Mustarelli P, Tomasi C, Quartarone E, Scavini M, Speghini A, Bettinelli M (2002) J Phys Chem B 106:9802
- El-Desoky MM (2010) Mater Chem Phys 119:389
- Garbarczyk JE, Jozwiak P, Wasiucionek M, Nowinski JL (2006) Solid State Ion 177:2585
- Garbarczyk JE, Jozwiak P, Wasiucionek M, Nowinski JL (2007) J Power Sources 173:743
- El-Desoky MM, Ibrahim FA, Mostafa AG, Hassaan MY (2010) Mater Res Bull 45:1122
- Al-Assiri MS, El-Desoky MM (2011) J Alloy Compd 509:8937
- El-Desoky MM, Al-Assiri MS (2007) Mater Sci Eng 37:237
- Austin IG, Mott NF (1969) Adv Phys 18:41
- Mott NF (1968) J Non Cryst Solids 1:1
- Sayer M, Mansingh A (1983) J Non Cryst Solids 58:91
- El-Desoky MM, Zayed HSS, Ibrahim FA, Ragab HS (2009) Phys B 404:4125
- Al-Assiri MS, Salem SA, El-Desoky MM (2006) J Phys Chem Solids 57:1873
- Al-Assiri MS, El-Desoky MM, Al-Hajry A, Al-Shahrani A, Al-Mogeeth AM, Bahgat AA (2009) Phys B 404:1437
- Holstein T (1959) Ann Phys 8:343
- Bogomolov VN, Kudinev EK, Firsov UN (1968) Sov Phys Solid State 9:2502